DOI 10.1007/s10891-022-02495-x
Journal of Engineering Physics and Thermophysics, Vol. 95, No. 2, March, 2022

FLOW DYNAMICS AND ACOUSTICS OF THE GAS JET EMANATING FROM A CONICAL NOZZLE INTO AN IMMERSED SPACE

K. N. Volkov,[a] V. N. Emel'yanov,[b] and P. S. Chernyshov[b] UDC 532.529

The subsonic and supersonic gas jets emanating from a conical nozzle into an immersed space were investigated. The influence of the difference between the total pressure at the inlet of the nozzle and the static pressure in the surrounding medium on the structure of such a jet and its flow dynamics and acoustics were determined and the noise level in the far field of the jet was calculated. The results of numerical simulation of the outflow of a gas from a conical nozzle into an immersed space were compared with the corresponding experimental and calculation data available in the literature. The methods developed for numerical simulation of the flow dynamics and acoustics of gas jets can be used for solving different research and engineering problems as well as for development of new computational algorithms.

Keywords: *computational gas dynamics and aeroacoustics, supersonic underexpanded jet, noise, conical nozzle.*

Introduction. Subsonic and supersonic gas jets are of frequent occurrence in rocket engines, audio-signal generators, production units, and technological processes used in the thermoacoustical working of metals, powder metallurgy, and steelmaking. The flow regime and structure of these jets and their gasdynamic behavior and acoustics can be controlled by different methods [1–3]. The noise produced by such a jet can be estimated using the direct noise computation (DNC) method, involving the simultaneous calculation of the noise generated by the turbulent structures in the jet and the propagation of sound waves beyond the region of turbulence of the jet as far as the position of an observer, as well as using the integral methods involving the separate calculations of the noise produced by a gas jet and the propagation of this noise. Of the last-mentioned methods the best known one is based on the Ffowcs Williams–Hawkings (FW–H) model.

Results of experimental and numerical investigations of supersonic jets and the noise generated by them are presented in [1–8]. From the practical standpoint, the main problems, whose solution calls for further investigations, is the intensification of the mixing of the gas, outflowing with a supersonic velocity from a nozzle, and the attenuation of the noise produced by the gas jet.

Despite the advances made in the simulation of turbulence and the development of aeroacoustic methods, the exact calculation of the noise characteristics of jet flows is still a difficult task. A modern approach to the calculation of the noise produced by a gas jet is based on the vortex-resolving simulation of the flow field of the jet with the use of Kirchhoff surfaces and an integral wave equation, e.g., the FW–H equation, for the description of the far acoustic field outside the jet.

The present work is devoted to computational simulation of the flow dynamics and acoustics of the subsonic and supersonic gas jets emanating from a conical nozzle into an immersed space with regard for the mode composition of the noise produced by them and the direction of its propagation.

Computational Region. A gas (air) jet emanating from an axisymmetric conical nozzle with an exit section of diameter $d_a = 76.20$ mm and a half-opening angle $\theta_a = 25^o$ (Fig. 1) into an immersed space is considered. The inner diameter of the cylindrical section of the nozzle is $d_{in} = 145.48$ mm, and its outer diameter is $d_{out} = 185.20$ mm. The ratio between the total pressure at the inlet cross section of the nozzle and the static pressure in the surrounding medium (the nozzle pressure ratio) NPR $= p_0/p_\infty$ was changed from 1.4 to 7 by changing the total pressure at the inlet cross section of the nozzle.

The problem on the outflow of a gas from a conical nozzle into an immersed space was solved in the axisymmetric approximation in the Cartesian coordinate system in which the line $y = 0$ corresponded to the symmetry axis of the nozzle. The computational region represented the rectangle $[0, L_x] \times [0, L_y]$ of size $80d_a$ downstream from the nozzle exit section,

[a]Kingston University, SW15 3DW, London, Great Britain; [b]D. F. Ustinov Baltic State Technical University "VOENMEKH", 1 1st Krasnoarmeiskaya Str., St. Petersburg, 190005, Russia; email: dsci@mail.ru. Translated from Inzhenerno-Fizicheskii Zhurnal, Vol. 95, No. 2, pp. 416–427, March–April, 2022. Original article submitted October 1, 2020.

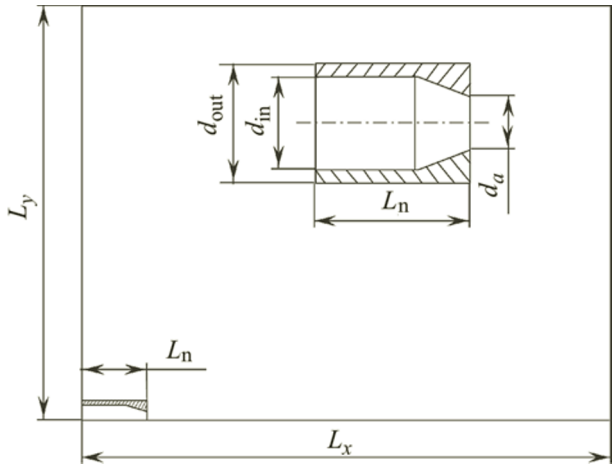

Fig. 1. Computational region and geometry of the nozzle.

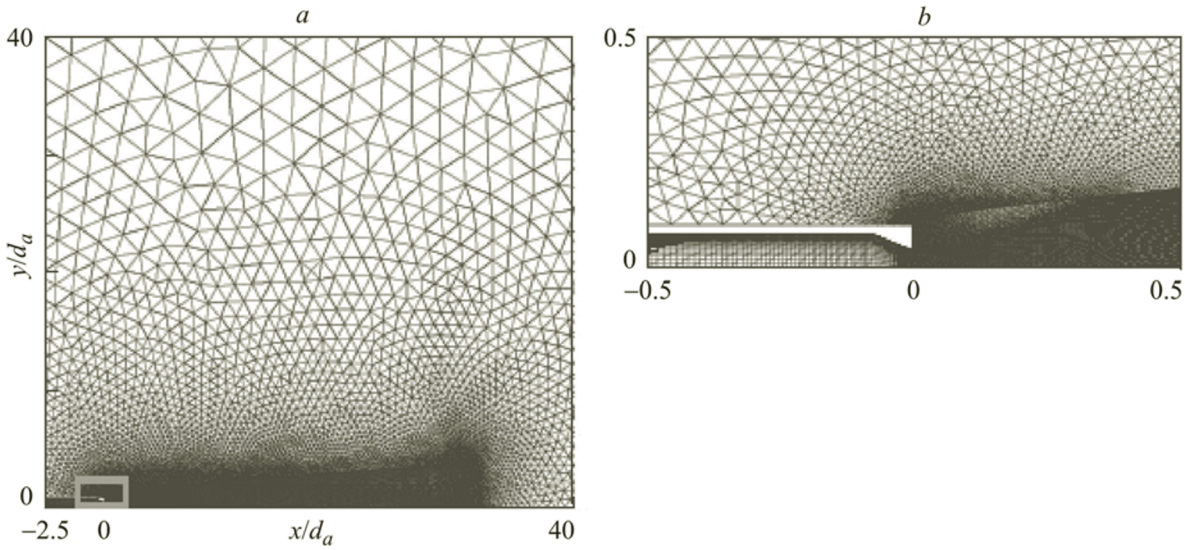

Fig. 2. Computational mesh (a) and its fragment near the nozzle exit section (b).

$10d_a$ upstream from it (this distance is equal to the length of the nozzle region of the jet L_n, including the lengths of the cylindrical and conical parts of the nozzle), and $35d_a$ in the radial direction [9–12]. The calculations were performed on the hybrid block mesh comprising triangular and quadrangular elements (Fig. 2). The quadrangular elements, forming the structured part of the mesh, were used inside the nozzle and in the region of outflow of the gas from it at a distance of 20 gauges from the nozzle exit section. The triangular elements, forming the nonstructured part of the mesh, were used in the region of the far field of the gas jet. The mesh used inside the nozzle was uniform in the direction of the gas flow (x axis) and nonuniform in the direction of the y axis with a bunching to the nozzle walls. The field of the air flow in the nozzle was calculated on the mesh containing 200 × 80 nodes. The mesh step along the radial coordinate near the nozzle wall comprised $2.54 \cdot 10^{-5}$ m (in this case, $y^+ \sim 1.8$). The mesh used in the region downstream of the nozzle exit section contained about 350 nodes along the axial coordinate and about 200 nodes in the radial direction. The refinement of the mesh near the jet flow provided an adequate resolution of the instability waves in the shear layer of the jet, its shock-wave structure, and the acoustic waves propagating in the near field of the jet. The computational mesh was coarsed in the direction to the outer boundaries of the computational region.

At the initial instants of time, the velocity profile of the gas flow along the longitudinal coordinate as well as the density and temperature of the gas in the jet were prescribed. At the input boundary of the computational region, the total

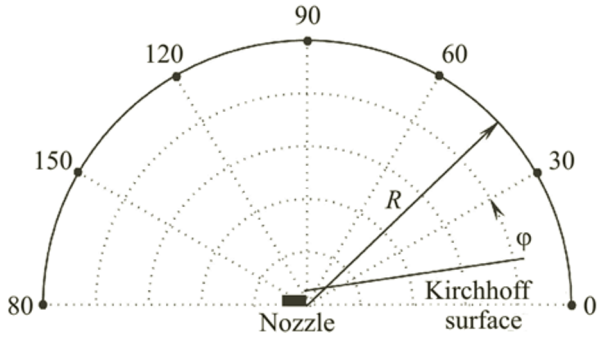

Fig. 3. Disposition of the observation points relative to the nozzle exit section.

pressure of the gas p_0, corresponding to the pressure in the settling chamber of the nozzle, and its total temperature T_0, corresponding to the temperature of stagnation of the gas flow in the settling chamber (T_0 = 288 K), were predetermined. The initial turbulence of the gas outflowing from the nozzle comprised 0.1% of the intensity of pulsations of the gas flow in the nozzle, and the ratio between the viscosity of the turbulent gas flow and the viscosity of the laminar gas flow was equal to unity. The pressure and temperature at the outer boundary of the computational region were $p_\infty = 10^5$ Pa and T_∞ = 288 K. The symmetry condition was set at the axis of the jet. The adhesion and impermeability conditions were prescribed for the gas at the inner and outer walls of the nozzle, and the adiabatic conditions were formulated for the temperature of the gas at these walls.

Calculation Method. The sound field of the gas jet emanating from a conical nozzle into an immersed space was calculated on the basis of the nonstationary Reynolds-averaged Navier–Stokes equations with the use of the k–ε turbulence model [13]. The results of calculations were compared with the corresponding results of experiments performed in [9, 12]. The field of vorticity of the gas jet was calculated by the large eddy simulation (LES) method [14–17], which made it possible to resolve only the large vortices in the jet determining the features of the gas flow in it, and the small vortices having a more universal structure were defined using the submesh turbulence model. The submesh viscosity of the gas was determined by the implicit LES (ILES) scheme, obtained as a results of the numerical dissipation of the computational LES scheme, because, in the calculation of the noise produced by the turbulent jet emanating from a nozzle within the framework of the LES scheme, of importance is the realistic description of the transformation of a laminar gas flow to the turbulent one in the mixing layer at the edge of the nozzle. At large Reynolds numbers, this process proceeds with a high rate determining the frequency range of the noise resolved by the LES scheme. The small-scale vortex structures, moving from the boundary layer at the wall of the nozzle and turbulizing the mixing layer at its edge, cannot be resolved within the framework of this scheme because of the high requirements imposed on the computational resources in it. As a rule, the use of classical (explicit) models of a submesh viscosity leads to a delay in the transition from a laminar flow to the turbulent one. This disadvantage can be eliminated by change of the real turbulent pulsations of the gas flow at the exit section of the nozzle to the artificial ones. The gas dynamics equations used in the calculations were discretized by the method of finite volumes [14]. The nonstationary gas dynamics equations were numerically solved using the method of integration with respect to the fictitious time, and as many as 25 iterations were performed to obtain a solution in each time layer. The basic equations were discretized with respect to the time by the implicit difference scheme of the second order of accuracy, and the MUSCL scheme of the third order of accuracy was used for discretization of these equations with respect to the space. The diffusion terms of the indicated equations were calculated by the difference scheme of the second order of accuracy. The time step comprised $5\cdot10^{-6}$ s, and it was determined by the experimental frequency characteristics of the process being considered. The parameters of a gas flow and of its turbulence, obtained by the LES method, were averaged and the noise produced by this flow was calculated using the statistic of time extent $300–1000 d_a/u_a$ corresponding to $(3–5)\cdot10^4$ time layers.

The sound pressure level of the gas jet emanating from a conical nozzle to an immersed space was determined by the nonstationary gasdynamic fields on the conical Kirchhoff surfaces surrounding the jet (Fig. 3), and the data obtained were used in the numerical integration of the inhomogeneous wave equation for calculating the sound pressure at definite observation points. The oscillation spectra of the pressure in the far acoustic field of the jet were determined on the basis of the fast Fourier transform with the use of the Hanning window. The spectra of the pressure oscillations in the azimuth direction were additionally averaged.

Results of Calculations. The outflow of a gas (air) from a converging conical nozzle into an immersed space was investigated depending on the difference between the total pressure at the inlet of the nozzle and the static pressure in the surrounding medium.

Structure of a gas jet. The flow dynamics of the initial region of the gas jet emanating from a conical nozzle into an immersed space is characterized by the presence of compression shocks, rarefaction waves, and a mixing layer. In the case where this jet is free, underexpanded, and supersonic, it has a characteristic shock-wave flow structure comprising a suspended compression shock, a reflected shock, a Mach disk, a boundary layer, and a layer formed downstream of the triple point of intersection of the shocks.

The lines of the Mach numbers of the gas outflowing from the nozzle, calculated for different nozzle pressure ratios, are shown in Fig. 4. At an NPR falling within the range from 1.4 to 1.8, the gas flow is subsonic, and, when NPR increases to 2, the gas flow becomes supersonic (for air, the critical nozzle pressure ratio is equal to 1.9). In Fig. 4e representing the case where NPR = 4, a Mach disk is well seen. When NPR increases, this disk increases and tends to shift downstream. In the initial region of the jet there arises a system of shocks (diamonds) which becomes nonstationary with time, and the shear layers at the boundaries of the jet downstream of the diamond which is third from the nozzle exit section are transformed into the almost isolated vortex structures. A comprehensive analysis of these structures and of the pressure and density fields in the gas jet has shown that the nonstationary shock waves in the third diamond penetrate to the gaps between the continuous shear layers retained and the neighboring vortex structures, with the result that compression waves are formed outside the jet. These waves propagate upstream in the form of semicircles and reach the nozzle exit section.

Results of calculations of the flow field of the gas jet emanating from a conical nozzle at NPR = 4, processed in the form of the absolute values of the density gradients of the gas flow, are compared with the shadow graph of such a jet, obtained in [12], in Fig. 5. A shock wave propagates through the two to three mesh cells, and a compression shock intersects with the axis of the jet at $x/d_a = 1.23$. The calculated angle of inclination of the compression shock to the jet axis comprises 49^o which coincides with that (49^o) given by the physical experiment [11].

Results of calculations of the parameters of the stationary supersonic nonisobaric gas jet, emanating from a conical nozzle, fairly well define the main features of its structure. The numerical simulation of such a jet is restricted by the flow models involved in it and, therefore, gives no way of defining the physical processes proceeding in the jet in the case where in it there arise vortex flows due to the curvature of the stream lines, the roughness of the inner surface of the nozzle, the initial turbulence of the gas flow, and other factors, but it allows one to fairly satisfactorily reproduce the qualitative pattern of the shock-wave structure of the jet.

Local characteristics of a gas jet. The distributions of Mach numbers of the supersonic gas jet emanating from a conical nozzle and the kinetic energy of turbulence along the jet axis are shown in Fig. 6. At the outlet of the nozzle there arises a system of compression shocks. The structure of the gas flow at the axis of the jet is cellular, and the distribution of the flow velocity in the jet has minima and maxima. The alternation of these maxima and minima determines the positions of the first and second cells in the jet, and the minima of the flow velocity correspond to the boundaries of the cells. At a distance from the nozzle exit section, equal approximately to its ten diameters, the shocks decay, and the Mach numbers decrease downstream along the axial coordinate. Turbulence is generated in the shear layer of the jet. The energy of turbulence near the edge of the nozzle is substantially increased because of the large flow-velocity gradients at it. Downstream from the nozzle exit section, where the velocity of the gas flow decreases as a result of its mixing with the surrounding air, the profile of the kinetic energy of turbulence is smoothed out gradually, and this energy decreases. The distributions of Mach numbers of the gas jet over its different cross sections are shown in Fig. 7. It is seen that the calculation and experimental data on this jet are in good agreement.

The gas flow in a conical nozzle is nonuniform. To determine the shape of the sound line of the gas jet emanating from such a nozzle and to compare it with the experimental one determined by the results of measuring the static pressure at the wall of the nozzle and at the axis of the jet [9], we calculated the Mach number

$$M_\omega = \left\{ \left(\frac{2}{\gamma - 1} \right) \left[\left(\frac{p_0}{p_\omega} \right)^{(\gamma-1)/\gamma} - 1 \right] \right\}^{1/2}.$$

The value of $M_\omega = 1.0$ corresponds to the position of the sound line on the nozzle wall (a supersonic gas flow is realized at NPR > 2).

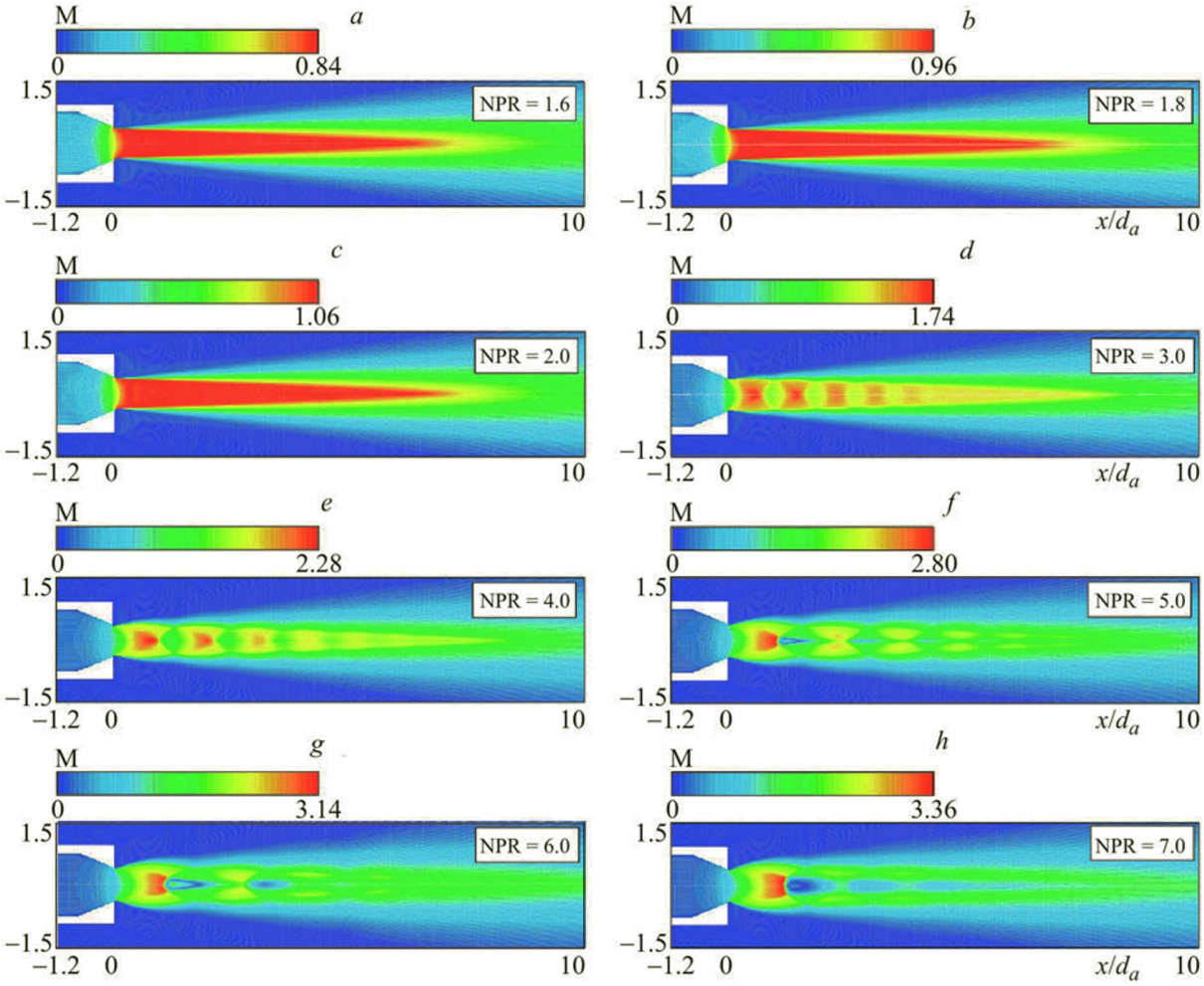

Fig. 4. Levels of the Mach numbers of the gas jet at NPR = 0.6 (a), 1.8 (b), 3 (d), 4 (e), 5 (f), 6 (g), and 7 (h).

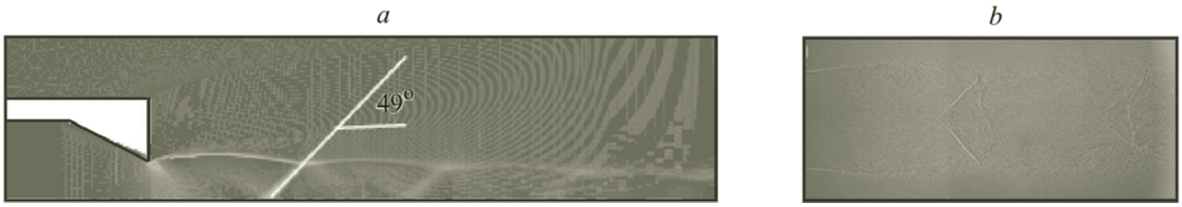

Fig. 5. Numerical pattern (a) and experimental shadowgraph (b) of the gas flow at NPR = 4.

The sound lines corresponding to different nozzle pressure ratios are shown in Fig. 8. The sound line, coincident with the axis of the jet, is at a distance of the order of half radius of the nozzle from its outlet cross section. As the NPR increases, the sound line moves to the nozzle exit section. When the NPR exceeds any critical value, the shape and position of the sound line cease to change, and the flow rate remains practically unchanged. The critical nozzle pressure ratio, used in the calculations, was $NPR_* = 4$ which fairly well agrees with the results of the physical experiment [9].

Discharge and thrust coefficients of a nozzle. The discharge and thrust coefficients of a conical nozzle were calculated and were compared with the corresponding experimental and calculation data available in the literature. The discharge coefficient of a conical nozzle differs from unity because of the inhomogeneous distribution of the parameters

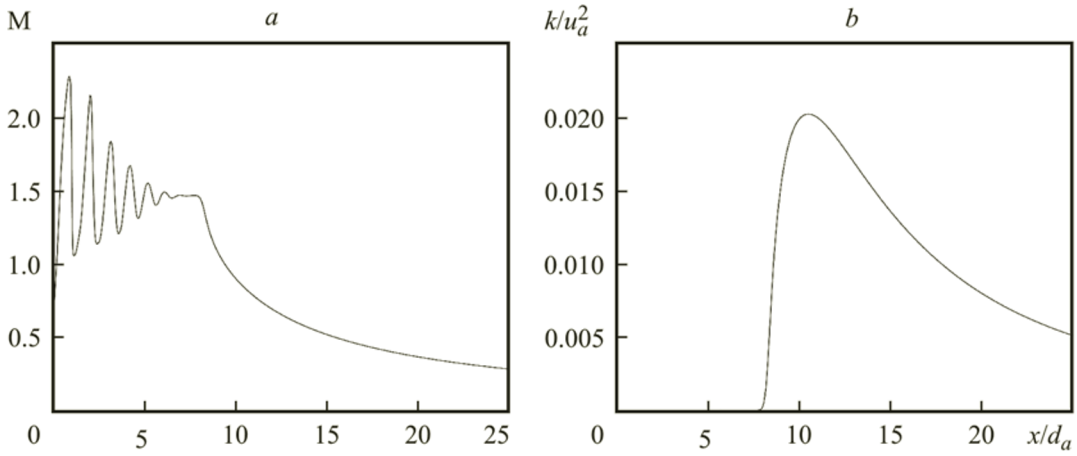

Fig. 6. Distributions of the Mach numbers of the gas jet (a) and the kinetic energy of turbulence (b) along the jet axis at NPR = 4.

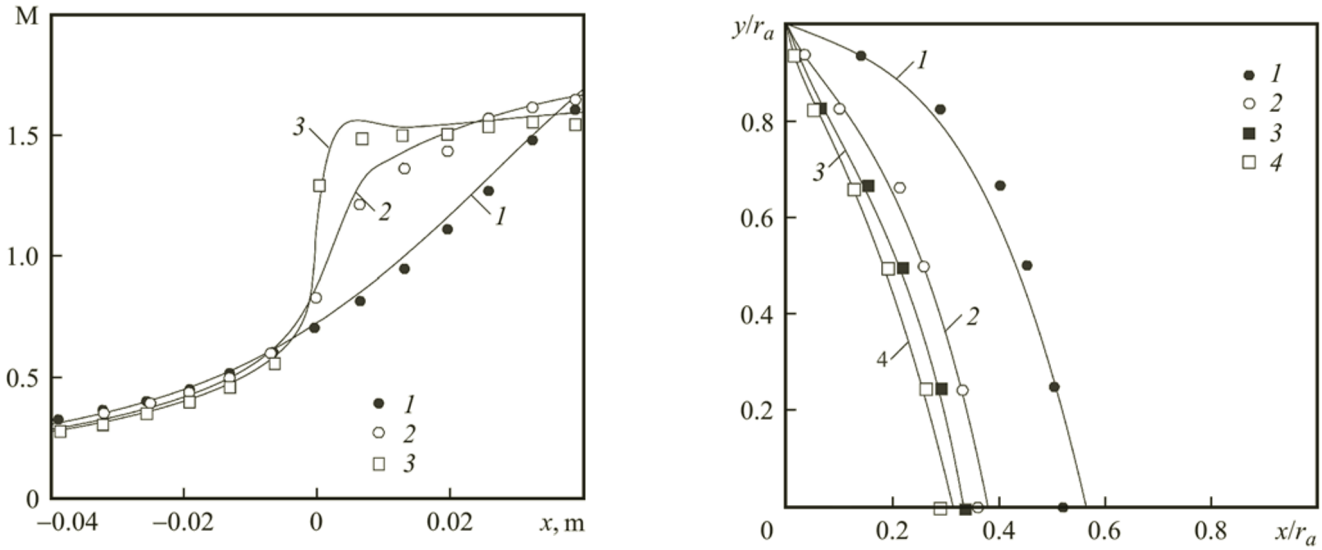

Fig. 7. Distributions of the Mach numbers of the gas jet, emanating from a conical nozzle with NPR = 4, over its cross sections at y = 0 (1), 31.75 (2), and 38.10 mm (3): full lines, calculation; points, results of the physical experiment.

Fig. 8. The shape of the sound lines at NPR = 2 (1), 2.5 (2), 3 (3), and 4 (4): full lines, calculation; points, results of the physical experiment.

of the gas flow over its outlet cross section and the presence of boundary layers at the nozzle walls [15]. The discharge coefficient of the nozzle was determined as the ratio between the real mass rate of the gas flow in it G and the ideal one G_j realized in the case of isentropic outflow of the gas from the nozzle under identical conditions: $G_D = G/G_j$. The discharge coefficient of the nozzle was calculated by the formula

$$C_D = \frac{2\pi \int_0^{r_a} \rho u r dr}{\rho_j U_j A_j},$$

where A_j is the area of the outlet cross section of the nozzle, and U_j is the velocity of the gas flow at it. The ideal mass flow rate of the gas was determined using the relations of the one-dimensional nozzle theory [15]

$$G_j = \frac{p_0 A_j}{(RT_0)^{1/2}} \left\{ \frac{2\gamma}{\gamma - 1} \left[\left(\frac{p_a}{p_0} \right)^{2/\gamma} - \left(\frac{p_a}{p_0} \right)^{(\gamma+1)/\gamma} \right] \right\}^{1/2} ,$$

where $p_a = p_\infty$. In the case of isentropic outflow of the gas from the nozzle, its mass flow rate increases with increase in the pressure at the inlet of the nozzle. When the critical nozzle pressure ratio

$$\mathrm{NPR}_* = \left(\frac{2}{\gamma + 1} \right)^{-\gamma/(\gamma-1)}$$

is attained, the gas mass flow rate reaches a maximum value determined by the formula

$$G_{j\max} = \frac{p_0 A_j}{(RT_0)^{1/2}} \left[\frac{2\gamma}{\gamma + 1} \left(\frac{2}{\gamma + 1} \right)^{2/(\gamma-1)} \right]^{1/2} .$$

A further increase in the pressure ratio of the nozzle causes no change in the rate of the mass flow in it. The critical pressure ratio of the nozzle depends on only the adiabatic index of the gas flowing in it, and $\mathrm{NPR}_* = 1.89$ for air ($\gamma = 1.4$). The critical pressure ratio of the nozzle corresponds to the establishment of a local velocity of sound at its outlet cross section. The calculations of the gas outflow from the nozzle at NPR = 1.4, 1.6, and 1.8 correspond to its subcritical regimes in which the ideal rate of the gas flow in the nozzle is realized at these values of NPR. The other calculations, performed for larger pressure ratios of the nozzle beginning with $\mathrm{NPR}_* = 1.9$, correspond to the supercritical regimes of gas outflow from it in which the gas jet formed is underexpanded, and the ideal rate of the gas flow in the nozzle reaches a maximum value if this flow is isentropic.

The thrust coefficient of a nozzle is a criterion of its internal losses and the losses that are due to the noncalculated expansion of the gas in it. This coefficient is determined as the ratio between the real thrust of the nozzle P and its ideal thrust P_j corresponding to the complete expansion of the gas in the nozzle ($p_a = p_\infty$) and the absence of internal losses caused by the real-gas viscosity: $C_V = P/P_j$. The expression for calculating the thrust coefficient of the nozzle has the form

$$C_V = \frac{2\pi \int_0^{r_a} [\rho u^2 (p - p_\infty)] r dr}{U_j \int_0^{r_a} \rho u r dr} .$$

The ideal thrust of the nozzle is determined by the relation $P_j = GU_j$. The mass flow rate of the gas at the outlet cross section of the nozzle is calculated, and the velocity of its isentropic outflow from the nozzle is determined theoretically. In the case where the nozzle works in the noncalculated regime, the pressure at its exit section is not equal to the environmental pressure ($p_a \neq p_\infty$), and the thrust of the nozzle that is due to the outflow of the gas from it is determined by the integral quantity P_1 depending on the local distributions of the density of the gas and the velocity of its flow in the nozzle. The thrust of the nozzle which is due to its pressure ratio is determined as the product of the excess pressure at the nozzle exit section into its area: $P_2 = A(p_a - p_\infty)$.

The discharge and thrust coefficients of a conical nozzle were determined by integration of the local distributions of the density of the gas and the velocity of its flow at the outlet cross section of the nozzle over the radial coordinate. The parameters of the isentropic gas flow in the nozzle with an outlet cross section of area $A_j = 322.35$ mm^2 were determined by the relations

$$U_j = M_j (\gamma R T_j)^{1/2} , \quad M_j = \left[\left(\frac{2}{\gamma - 1} \right) (\mathrm{NPR}^{(\gamma-1)/\gamma} - 1) \right]^{1/2} , \quad T_j = T_0 \left[1 + \left(\frac{\gamma - 1}{2} \right) M_j^2 \right]^{-1} .$$

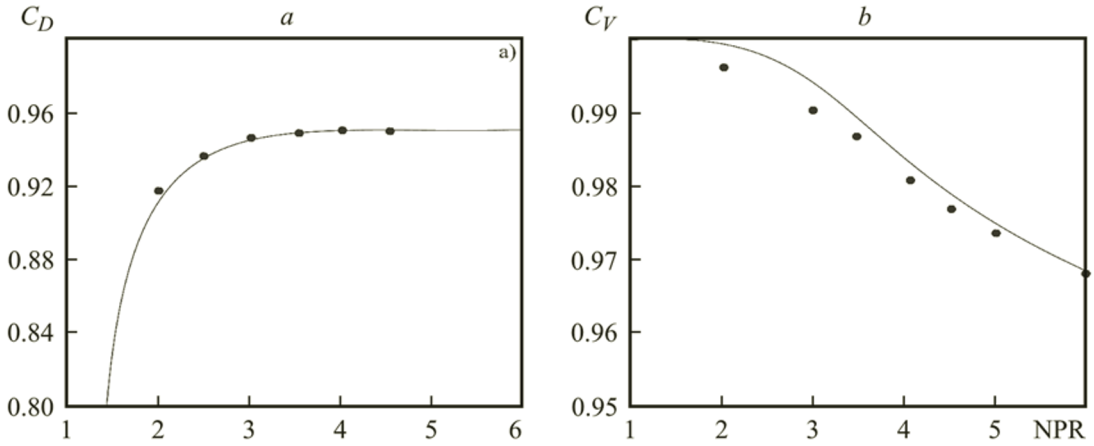

Fig. 9. Dependence of the discharge (a) and thrust (b) coefficients of a conical nozzle on its pressure ratio.

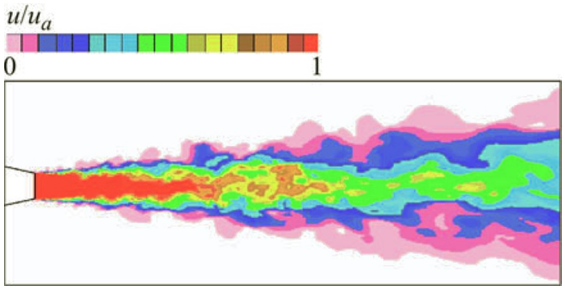

Fig. 10. Instantaneous velocity field of a steady gas jet.

The dependences of the discharge and thrust coefficients of the conical nozzle being considered on its pressure ratio are shown in Fig. 9. It is seen that the calculation data on these coefficients and the experimental ones obtained in [12] are in good agreement. The discharge coefficient of the nozzle increases sharply with increase in its pressure ratio to two, and then it remains approximately unchanged. The discharge coefficient of the nozzle remains approximately unchanged at small values of the pressure ratio of the nozzle, and it decreases by 4–5% with increase in this ratio. Whereas the calculation and experimental data on the discharge coefficient of the nozzle are in good agreement, the calculations of the thrust coefficient of the nozzle give its values overestimated by 1–1.5% compared to those obtained in the experiment.

Generation of noise. The acoustic noise in the far field of the compressed turbulent jet emanating from a converging conical nozzle into an immersed space was calculated. The main constitutive parameters of the problem are the Mach number of the completely expanded jet and its Reynolds number. At M_a = 09, the Reynolds number of the jet, determined by its parameters at the nozzle exit section, is equal to $Re = 1.2 \cdot 10^6$. The instantaneous velocity field of a steady gas jet is shown in Fig. 10, and the instantaneous pressure field in this jet, represented in the scales of its flow dynamics and acoustics, is shown in Fig. 11. In the acoustic pressure distribution, the low-frequency waves are well defined.

The sound pressure at a large distance from the nozzle was calculated using the acoustic analogy method, in accordance with which a special surface surrounding the jet from the outside was separated in the computational region, and the velocity, density, and pressure fields of the gas flow on this surface were determined. The data obtained were than processed with the use of a special subprogram for calculating the FW–H integral. The noise level of the gas jet was determined at the points, positioned at a distance r/d_a = 98 from the nozzle exit section for the vectorial angles 20–160°. The data obtained were additionally averaged over the ten azimuth angles. The third-octave spectra of the noise in the far field of the gas jet are compared with the corresponding experimental data obtained in [20] in Fig. 12, and the directivity diagrams of the integral noise of the gas are compared with the experimental ones obtained in [20] and [21] in Fig. 13. The calculation and experimental data, obtained for the Strouhal numbers of the jet $0.2 < St < 1.5$, are in satisfactory agreement.

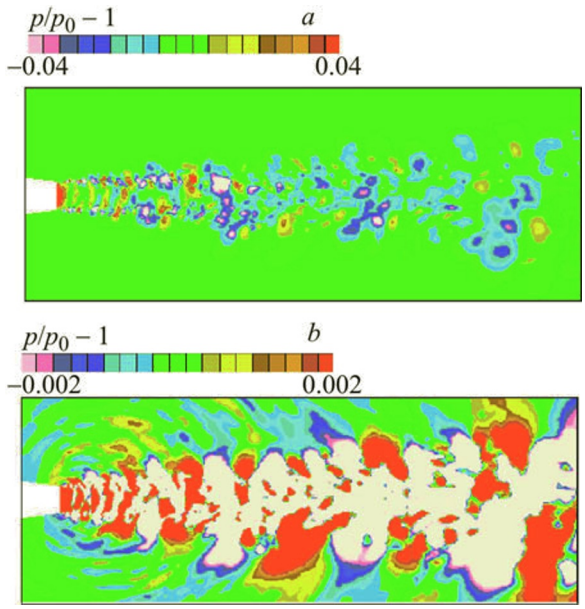

Fig. 11. Instantaneous pressure fields of a steady gas jet represented in the scales of its flow dynamics (a) and acoustics (b).

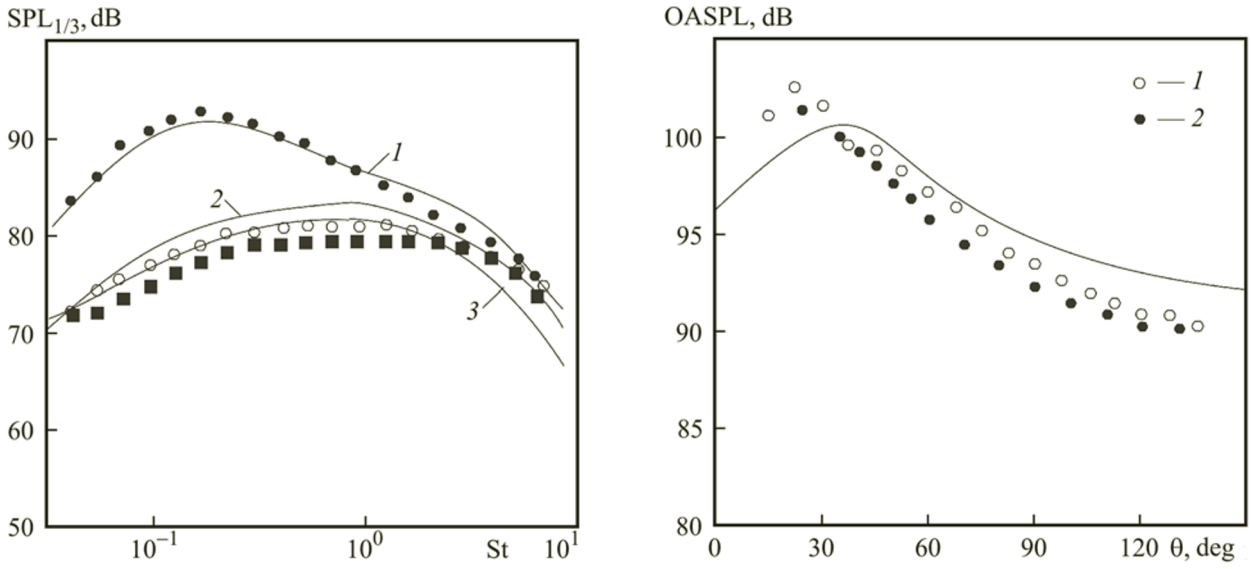

Fig. 12. Comparison of the third-octave spectra of the noise of a gas jet in its far field calculated for φ = 30 (1), 90 (2), and 120° (3) (full lines) with the corresponding experimental data [20] (points).

Fig. 13. Calculated directivity diagrams of the integral noise of a gas jet (full line) and experimental ones obtained in [20] (1) and [21] (2).

The frequency distribution of the sound level of the gas jet is fairly homogeneous with a certain bias to the side of higher frequencies, and the integral level of this pressure (OASPL) corresponds to the experimental one.

The calculated dependences of the integral pressure of the subsonic gas jet emanating from a conical nozzle with r/d_a = 53 on its angular coordinate and Mach number are compared with the corresponding experimental data [18] in

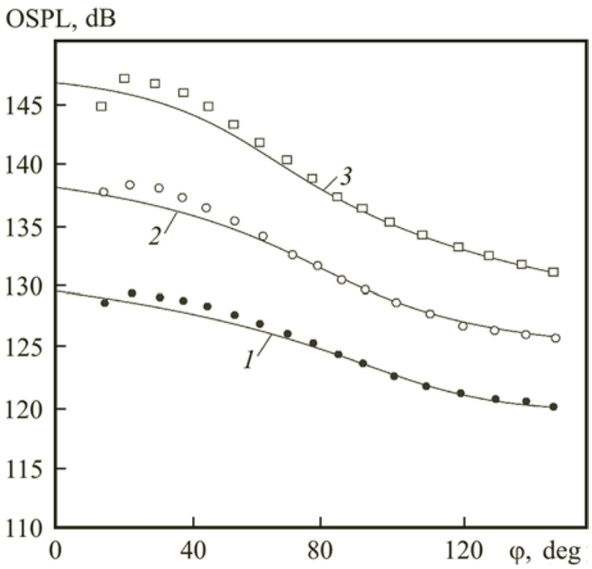

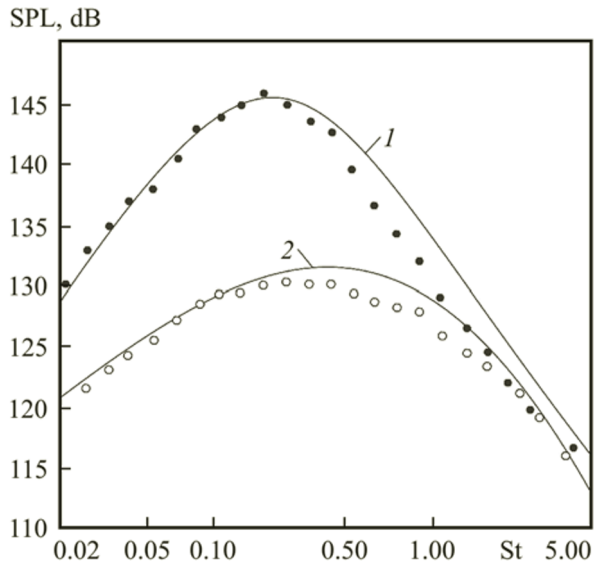

Fig. 14. Dependence of the integral sound pressure of a gas jet on its angular coordinate at M = 0.6 (1), 0.75 (2), and 0.9 (3).

Fig. 15. Frequency distribution of the sound pressure of a gas jet at φ = 30 (1) and 90° (2).

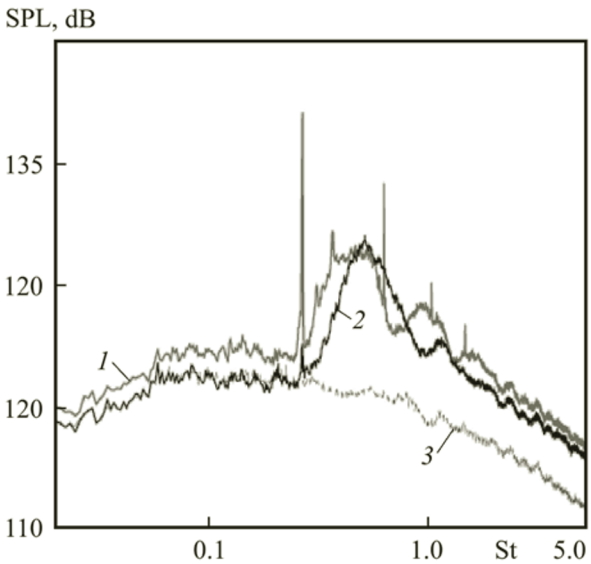

Fig. 16. Spectra of the sound pressure of the gas jets emanating from a conical nozzle (1) and a corrugated nozzle (2, 3) [19] at M = 1.3.

Fig. 14. The frequency distributions of the sound pressure of such a gas jet with M = 0.75 at the nozzle exit section, calculated for its different angular coordinates, are compared with the experimental ones in Fig. 15.

The noise of a supersonic nonisobaric gas jet emanating from a conical nozzle has three components: the turbulent-mixing noise, the broadband shock-wave noise, and the discrete-tone noise. The mixing noise is emitted by the turbulent structures in the form of Mach waves, moving in the mixing layer of the jet and interacting with the surrounding medium, to the environment due to the supersonic velocity of the convective motion of the gas in the jet. Depending on the wave number of the sound, it can be emitted from different regions of the jet along its length and at different angles because of the different attenuation and amplification coefficients of individual vortex structures. The shock-wave noise appears in the

noncalculated regimes of outflow of the gas from the nozzle. This noise is emitted as a result of the increase in the amplitude of vibrations of large-scale vortex structures in the process of their passage through the normal and oblique compression shocks in the gas jet. In the case of passage of a vortex through a compression shock downstream from the front of a shock wave, the pressure in one part of the vortex increases, and the pressure in its other part decreases, with the result that compression and rarefaction waves are formed. These waves propagate in different directions, and the system as a whole behaves like a dipole radiation source. The power of the shock-wave noise produced by a gas jet is directly related to its kinetic energy, and the discrete-tone noise of the jet is related to its shock-wave noise. A discrete-tone noise is produced by a supersonic nonisobaric gas jet mainly due to the existence of an acoustic feedback in it. The noise emitted from the boundaries of the shock-wave diamonds in the jet propagates in the direction opposite to the direction of propagation of the jet and acts in the thin mixing layer formed near the nozzle exit section, which enhances the disturbances taking place in the self-vibrating system and gives rise to definite-frequency vibrations of the gas in it (discrete tones appear in the noise spectrum of the jet). The intensity of the discrete-tone noise of a gas jet depends on its Mach number and temperature, the size of the nozzle exit section, and the parameters of the surrounding medium because of the presence of an acoustic feedback in the jet.

An intense discrete-tone sound produced, by the noncalculated supersonic gas jet, emanating from a conical nozzle, as a result of the activation of an acoustic feedback by a quasiperiodic shock-wave structure in it, represents the main noise of this jet. An acoustic wave, propagating upstream in such a jet, interacts with the edge of the nozzle and initiates instability waves in the thin mixing layer at the nozzle outlet. These waves are transported downstream with increase in their amplitude and interact with a periodic shock-wave structure, with the result than an acoustic wave is generated. This wave propagates upstream outside the jet in the direction to the nozzle exit section, and, when it reaches this section, a new instability wave is formed, and the loop is closed. The frequency of the discrete-tone sound produced by the jet is determined by the phase velocity of the disturbances of the gas in it and by the wavelength of the jet instability possessing its own dynamics.

The spectra of the sound pressure of the supersonic gas jets emanating from a converging conical nozzle ($r/d_a = 52$) at $\varphi = 110^o$, a corrugated nozzle, and a Loval nozzle are shown in Fig. 16. The use of corrugated nozzles makes it possible to suppress the screech-effect [19].

Conclusions. The outflow of a gas from a conical nozzle was numerically simulated, and it was shown that the nozzle pressure ratio influences the shock-wave structure of the gas jet formed and the distribution of the parameters of the jet along its axis. A comparison of the results of calculations of such a jet with regard for the nozzle pressure ratio with the results of corresponding experiments has shown that the calculation data obtained represent the shock-wave structure of this gas jet fairly well and that the calculated local and integral parameters of the gas flow in the jet agree well with those obtained in the physical experiment. The results of our calculations of the supersonic gas jet emanating from a conical nozzle allow one to reproduce the broadband noise, produced by the shock-wave cells in this jet, which propagates mainly sideward and upstream, as well as the noise that is due to the turbulent mixing of the gas in the end region of the jet. The numerical simulation methods proposed can be used for calculating nonstationary three-dimensional turbulent flows of a compressible viscous gas and the acoustic effects arising in the case of outflow of this gas from a conical nozzle into an immersed space.

NOTATION

C_D and C_V, discharge and thrust coefficients of a conical nozzle; d_a, diameter of the nozzle exit section, m; G, rate of a mass gas flow, kg/s; k, kinetic energy of turbulence, m^2/s^2; M, Re, and St, Mach, Reynolds, and Strouhal numbers; p_a and p_∞, total pressure at the inlet cross section of the nozzle and the static pressure in the surrounding medium, Pa; r, radius of a gas jet, m; R, gas constant, J/(kg·K); T, temperature of the gas, K; u_a, velocity of outflow of the gas from the nozzle, m/s; x and y, Cartesian coordinates, m; γ, ratio between the specific heat capacities of the gas at a constant pressure and a constant volume; ε, rate of dissipation of the kinetic energy of turbulence, m^2/s^3; θ, half-opening angle of the nozzle, deg; ρ, density of the gas, kg/m^3; φ, vectorial angle, deg. Subscripts: in, inner; max, maximum; n, nozzle; out, outlet; w, wall; 0, stagnation parameter; +, dimensionless parameter near the nozzle wall; *, critical parameter; 1.3, third-octane parameter.

REFERENCES

1. V. G. Dulov and G. A. Luk'yanov, *Gas Dynamics of Outflow Processes* [in Russian], Nauka, Novosibirsk (1984).
2. G. Raman, Supersonic jet screech: Half-century from Powell to the present, *J. Sound Vib*., **225**, No. 3, 543–571 (1999).

3. A. S. Ginevskii, B. V. Vlasov, and R. K. Karavosov, *Acoustical Control of Turbulent Jets* [in Russian], Fizmatlit, Moscow (2001).
4. V. G. Pimshtein, Occurrence and development of vortices in turbulent jets under the effect of sawtooth sound waves of finite amplitude, *J. Eng. Phys. Thermophys*., **75**, No. 2, 277–280 (2002).
5. S. A. Isaev, Yu. M. Lipnitskii, P. A. Baranov, A. V. Panasenko, and A. E. Usachov, Simulation of a turbulent supersonic underexpanded jet flowing into a submerged space with the help of a shear stress transfer model, *J. Eng. Phys. Thermophys*., **85**, No. 6, 1357–1371 (2012).
6. C. Chin, M. Li, C. Harkin, T. Rochwerger, L. Chan, and A. Ooi, Investigation of the flow structures in supersonic free and impinging jet flows, *J. Fluids Eng*., **135**, No. 3, Article ID 031202 (2013).
7. K. N. Volkov, V. N. Emel'yanov, and V. A. Zazimko, *Turbulent Jets: Static Models and Simulation of Large Votrices* [in Russian], Fizmatlit, Moscow (2014).
8. V. Zapryagaev, N. Kiselev, and D. Gubanov, Shock-wave structure of supersonic jet flows, *Aerospace*., **5**, 60–78 (2018).
9. R. L. Thornock and E. F. Brown, An experimental study of compressible flow through convergent-conical nozzles, including a comparison with theoretical results, *ASME J. Basic Eng*., **94**, No. 4, 926–932 (1972).
10. N. Spotts, S. Guzik, and X. Gao, A CFD analysis of compressible flow through convergent-conical nozzles, *AIAA Paper*, No. 2013–3734 (2013).
11. R. L. Thornock and J. S. Sokhey, Propulsion aerodynamic workshop. Comparison of participant analyses with experimental results for convergent conical nozzle flow fields and performance, *AIAA Paper*, No. 2013–3735 (2013).
12. V. F. Dippold, *Computational Simulations of Convergent Nozzles for the AIAA 1st Propulsion Aerodynamics Workshop*, NASA Report, No. TM-2014-218329, 2014.
13. A. T. Thies and C. K. W. Tam, Computation of turbulent axisymmetric and nonaxisymmetric jet flows using the k–ε model, *AIAA J.*, **34**, No. 2, 309–316 (1996).
14. K. N. Volkov, V. N. Emel'yanov, A. I. Tsvetkov, and P. S. Chernyshov, Mechanisms of generation of noise by supersonic jets and numerical simulation of their gasdynamic and acoustic characteristics, *Vych. Metody Program*., **20**, No. 1, 498–515 (2019).
15. M. M. A. Alam, T. Setoguchi, S. Matsuo, and H. D. Kim, Nozzle geometry variations on the discharge coefficient, *Propuls. Power Res*., **5**, No. 1, 22–33 (2016).
16. V. N. Emelyanov, A. I. Tsvekov, and K. N. Volkov, Mechanisms of generation and sources of noise in supersonic jets, *J. Akustika*, **32**, 144–150 (2019).
17. P. Chernyshov, V. Emelyanov, A. Tsvekov, and K. Volkov, Large-eddy simulation of noise generated by pulsed supersonic jets, *J. Akustika*, **34**, 137–141 (2019).
18. C. Bogey, S. Barre, V. Fleury, C. Bailly, and D. Juve, Experimental study of the spectral properties of near-field and far-field jet noise, *Int. J. Aeroacoust*., **6**, No. 2, 73–92 (2007).
19. B. Andre, T. Castelain, and C. Bailly, Broadband shock-associated noise in screeching and non-screeching underexpanded supersonic jets, *AIAA J.*, **51**, No. 3, 665–673 (2013).
20. K. Viswanathan, Aeroacoustics of hot jets, *J. Fluid Mech*., **516**, 39–82 (2004).
21. H. K. Tanna, An experimental study of jet noise. Part I. Turbulent mixing noise, *J. Sound Vibr.*, **50**, 405–428 (1977).